Antiviral Research 92 (2011) 424–433

Contents lists available at SciVerse ScienceDirect

Antiviral Research

journal homepage: www.elsevier.com/locate/antiviral

Exploring the molecular basis of dsRNA recognition by NS1 protein of influenza A virus using molecular dynamics simulation and free energy calculation

Dabo Pan [a], Huijun Sun [c], Yulin Shen [d], Huanxiang Liu [a,b,*], Xiaojun Yao [b,c]

[a] School of Pharmacy, Lanzhou University, Lanzhou 730000, China
[b] State Key Laboratory of Applied Organic Chemistry, Lanzhou University, Lanzhou 730000, China
[c] Department of Chemistry, Lanzhou University, Lanzhou 730000, China
[d] Gansu Computing Center, Lanzhou 730030, China

ARTICLE INFO

Article history:
Received 26 May 2011
Revised 23 September 2011
Accepted 23 September 2011
Available online 4 October 2011

Keywords:
Influenza A virus
Nonstructural protein 1
Protein–RNA interaction
Molecular dynamics simulation
Molecular mechanics generalized born surface area (MM-GBSA)

ABSTRACT

The frequent outbreak of influenza pandemic and the limited available anti-influenza drugs highlight the urgent need for the development of new antiviral drugs. The dsRNA-binding surface of nonstructural protein 1 of influenza A virus (NS1A) is a promising target. The detailed understanding of NS1A–dsRNA interaction will be valuable for structure-based anti-influenza drug discovery. To characterize and explore the key interaction features between dsRNA and NS1A, molecular dynamics simulation combined with MM-GBSA calculations were performed. Based on the MM-GBSA calculations, we find that the intermolecular van der Waals interaction and the nonpolar solvation term provide the main driving force for the binding process. Meanwhile, 17 key residues from NS1A were identified to be responsible for the dsRNA binding. Compared with the wild type NS1A, all the studied mutants S42A, T49A, R38A, R35AR46A have obvious reduced binding free energies with dsRNA reflecting in the reduction of the polar and/or nonpolar interactions. In addition, the structural and energy analysis indicate the mutations have a small effect to the backbone structures but the loss of side chain interactions is responsible for the decrease of the binding affinity. The uncovering of NS1A–dsRNA recognition mechanism will provide some useful insights and new chances for the development of anti-influenza drugs.

1. Introduction

As reported from the World Health Organization, the annual influenza epidemics result in about three to five million cases of severe illness and about 250,000–500,000 deaths. Especially, the outbreaks of the influenza A H5N1 and H1N1 in recent years, and the human fatalities they have already caused, have heightened the awareness of both the general population and governments to the threat of influenza virus. At present, there are only four effective anti-influenza virus drugs, namely amantadine, rimitadine, oseltamivir and zanamivir. Among them, the anti-influenza drugs amantadine and rimitadine target the M2 protein, a viral proton channel (Hay et al., 1985; Stouffer et al., 2008; Wang et al., 1993). However, a single residue change is sufficient to confer resistance, which has risen sufficiently to render the drug useless against many strains. Neuraminidase (NA) inhibitors including oseltamivir (Tamiflu) and zanamivir (Relenza) prevent viral particles being released from infected cells (Kim et al., 1997; Liu et al., 2007; Russell et al., 2006; von Itzstein et al., 1993). These two drugs are effective against 2009 influenza H1N1 virus (Hartley et al., 2009), while H5N1 virus is resistant to these drugs (de Jong et al., 2005; Hurt et al., 2009; Le et al., 2005; Mishin et al., 2005). At the same time, the resistant H1N1 influenza virus to oseltamivir is already emerging (Dharan et al., 2009; Moscona, 2009; Weinstock and Zuccotti, 2009). The effective anti-influenza drugs are still very lacking. Once a new influenza virus occurs, it is possible to face the state without effective drugs. To avoid such situation, it is urgent to seek novel anti-influenza virus drugs or novel therapeutic agents. For the development of anti-influenza virus drugs, the elucidation of the underlying mechanisms of viral replication and the understanding about influenza virus how to escape host defense are critical.

The NS1 protein of influenza A virus (NS1A protein), as a multifunctional protein that participates in both protein–RNA and protein–protein interactions (Chien et al., 2004; Hatada and Fukuda, 1992; Nemeroff et al., 1998; Noah et al., 2003), plays a critical role in countering host cell antiviral defenses (Hale et al., 2008; Krug et al., 2003) and is expected to play important roles in viral virulence (Das et al., 2008; Solorzano et al., 2005). This protein includes two domains, N-terminal domain ($NS1A_N$, residues 1–70) and C-terminal domain (known as the effector domain, residues 86–230/237). The $NS1A_N$ binds to double-stranded RNA (dsRNA)

* Corresponding author at: School of Pharmacy, Lanzhou University, Lanzhou 730000, China. Tel./fax: +86 931 8915686.
E-mail address: hxliu@lzu.edu.cn (H. Liu).

0166-3542/$ - see front matter © 2011 Elsevier B.V. All rights reserved.
doi:10.1016/j.antiviral.2011.09.009

and this dsRNA-binding activity is important to protect the viruses against human antiviral response during infection (Hale et al., 2008; Krug et al., 2003; Lu et al., 1995; Wang et al., 1999). In addition, one influenza A virus mutant strain that encodes NS1A protein with R38A mutation is highly attenuated (Cheng et al., 2009; Min and Krug, 2006), indicating that drugs interfering with $NS1A_N$–RNA binding should inhibit virus replication. The structural studies also revealed the NS1A dsRNA-binding site can be targeted for the development of antiviral directed against influenza A virus (Cheng et al., 2009; Das et al., 2010; Krug and Aramini, 2009).

Although the reported crystal structure of $NS1A_N$–RNA complex can provide plentiful atomic-level structural information to understand the structural basis of dsRNA recognition by NS1A, the molecular details of dsRNA recognition by NS1A are still unclear. Additionally, the experiments indicate (Cheng et al., 2009; Chien et al., 1997, 2004; Liu et al., 1997) the mutations of the residues on the concave dsRNA-binding surface, such as R35, R38, S42 and T49, which are directly related on dsRNA-binding, will highly reduce binding affinity with the dsRNA. Especially, dsRNA binding is abolished for the R38A single mutant and R35AR46A double mutant. Why and how do these mutants reduce or abolish dsRNA binding? To design the effective inhibitor, we need to understand the origin to affect the binding affinity of $NS1A_N$ and dsRNA, furthermore to know how to interfere their interactions for finding the effective compounds. In recent years, molecular dynamics (MD) simulations combined with binding free energy calculations have been used widely and successfully to study protein–protein, protein–RNA, and protein–DNA interactions (Liu and Yao, 2010; Rungrotmongkol et al., 2009; Sharon et al., 2011). This method can provide not only plentiful structural–dynamical information on protein complex structures in solution but also a wealth of energetic information, including the binding free energy between protein partners. Such information is very important to understand the essence of protein–protein or protein–RNA interactions and guide the drug design and development, whereas they cannot be provided by the experimental strategy.

In order to characterize and identify the key residues in the interaction between dsRNA and NS1A as well as to understand why the mutations of some residues such as S42, T49, R38, R35, and R46 result in the attenuation of dsRNA binding affinity by NS1A, 10 ns multiple trajectories molecular dynamics simulation and free energy calculation were performed on the wild type and mutated NS1A protein with dsRNA complexes. These simulations can complement experiments for better understanding of the NS1A–dsRNA molecular recognition mechanism by providing atomic details and conformational dynamics that are often inaccessible in experiment due to resolution limits. The detailed interaction profile from MD simulation and the molecular mechanics generalized born surface area (MM-GBSA) calculation will help us understand which features will determine the NS1A–dsRNA binding process as well as give some insights for structure-based inhibitors design.

2. Materials and methods

2.1. Molecular systems

The crystal structure of NS1A–dsRNA complex structure used in this study was taken from the Protein Data Bank (PDB ID: 2ZKO) (Cheng et al., 2009). In this crystal structure, $NS1A_N$ (residues 1–70) exists in a homodimeric state that binds double-stranded RNA (dsRNA, residues 1–21). Based on the wild type structure, several experimental reported mutants (Cheng et al., 2009) S42A, T49A, R38A, and R35AR46A double mutations which give a large effect to the binding affinity with dsRNA, were modeled by mutating the corresponding residues using Pymol program (DeLano, 2002) and the mutated residues were shown in Fig. 1. Two glycerol molecules and all the crystal water molecules were kept during the molecular dynamics simulation.

2.2. Molecular dynamics simulations

The molecular dynamics simulations including the energy minimization and equilibration protocols were performed by using AMBER 10.0 software package (Case et al., 2005). To keep the whole system neutral, Na^+ counter ions were added. Each system was then solvated using atomistic TIP3P water (Jorgensen et al., 1983) in a cubic box with at least 10 Å distance around the complex. Subsequently, to remove bad contacts, the system was minimized by using the steepest descent method switched to conjugate gradient every 1000 steps totally for 2000 steps with a 0.1 kcal/mol $Å^2$ restrains on all atoms. As follows, the system was gently heated from 0 to 300 K over a period of 50 ps by a Langevin thermostat with a coupling coefficient of 0.1/ps. The system was again equilibrated for 500 ps. The production phase of the simulations was run by releasing all the restrains for a total of 10 ns. In order to give the statistically reasonable results, three parallel simulations for each system were performed. Long-range Coulombic interactions were calculated using the particle mesh Ewald (PME) summation (Essmann et al., 1995) and the SHAKE algorithm (Ryckaert et al., 1977) was employed on all atoms covalently bonded to a hydrogen atom.

2.3. MM-GBSA calculation

Using the extracted snapshots from the equilibrated trajectories, the binding free energy calculations were performed by MM-GBSA method (Kollman et al., 2000). In this method, the binding free energy is computed as follows:

$$\Delta G_{\text{bind}} = G_{\text{complex}} - G_{\text{protein}} - G_{\text{RNA}}$$

Here, G_{complex}, G_{protein}, G_{RNA} are the free energies of complex, protein, and RNA, respectively. The free energy, G, for each species can be calculated by the following scheme using the MM-GBSA methods (Kollman et al., 2000):

$$G = E_{\text{gas}} + G_{\text{sol}} - TS$$
$$E_{\text{gas}} = E_{\text{int}} + E_{\text{ele}} + E_{\text{vdw}}$$
$$E_{\text{int}} = E_{\text{bond}} + E_{\text{angle}} + E_{\text{torsion}}$$
$$G_{\text{sol}} = G_{\text{sol-ele}} + G_{\text{sol-np}}$$
$$G_{\text{sol-np}} = \gamma \text{SASA}$$

Here, E_{gas} is the gas-phase energy; E_{int} is the internal energy; E_{bond}, E_{angle}, and E_{torsion} are the bond, angle, and torsion energies, respectively; and E_{ele} and E_{vdw} are the Coulomb and van der Waals energies, respectively. G_{sol} is the solvation free energy and can be decomposed into polar and nonpolar contributions. $G_{\text{sol-ele}}$ is the polar solvation contribution calculated by solving the GB equation (Kollman et al., 2000; Srinivasan et al., 1998). The dielectric constant of solvent was set as 80. The dielectric constant of solute was shown to be an important factor to influence the calculation of solvation free energy. Here, to select the proper dielectric constant of solute, different values (1, 2 and 4) were tried. When the dielectric constant of solute was set as 4, each parallel trajectory can give similar results and the reasonable binding free energies were obtained. Thus, the following discussions about binding free energy were based on the calculated results obtained by using 4 as the dielectric constant of solute. $G_{\text{sol-np}}$ is the nonpolar solvation contribution and is estimated by the solvent accessible surface area (SAS) determined using a water probe radius of 1.4 Å. The surface tension constant γ was set to 0.0072 kcal/mol $Å^2$ (Sitkoff et al.,

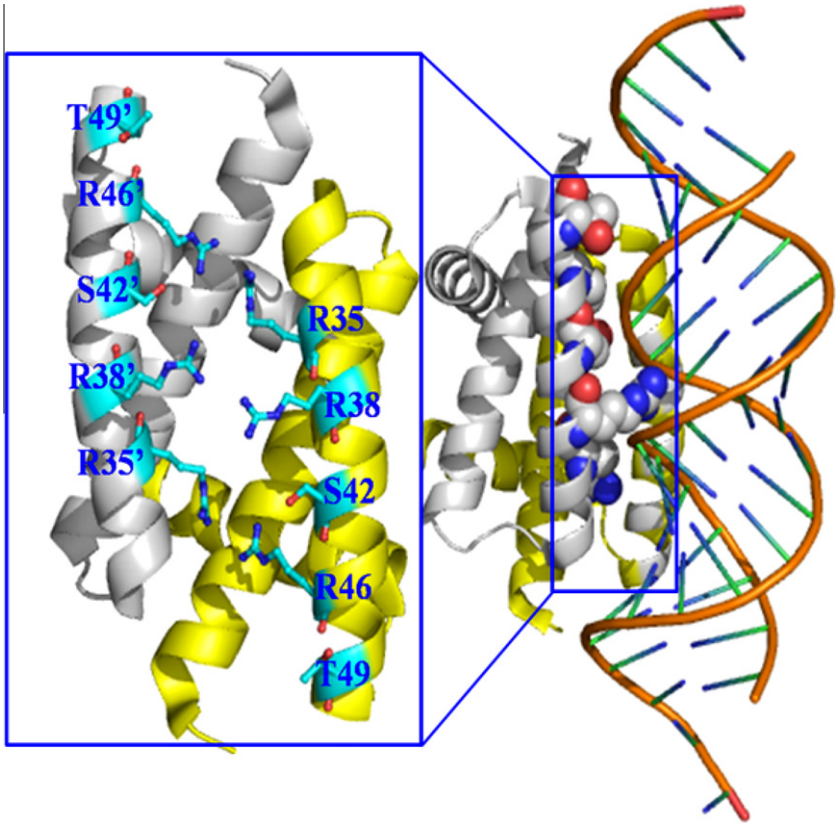

Fig. 1. The structure of the NS1A–dsRNA complex and the studied key mutations.

1994). The vibrational entropy (S) contributions were estimated by normal mode analysis (Chong et al., 1999). In this method, the frequencies of the normal modes are calculated from a molecular mechanics force field using the Hessian matrix of second energy derivatives in terms of the force constants for each type of interaction. This requires an input structure that is extracted from molecular dynamics trajectory and minimized by a Newton–Raphson protocol to obtain the Hessian matrix of second energy derivatives. Because of the high computational demand, only 20 snapshots were used in normal mode analysis for every trajectory and each snapshot was optimized for 100,000 steps using a distance-dependent dielectric of $4r_{ij}$ (r_{ij} is the distance between atoms i and j) until the root-mean-square deviation of the gradient vector was less than 0.0001 kcal/mol Å^2.

3. Results and discussion

3.1. Binding free energy calculation and the identification of key residues in wild type NS1A–dsRNA complex

The equilibration of molecular dynamics trajectories was monitored from the convergence of the root-mean square deviation (RMSD) of the backbone atoms of NS1A–dsRNA complexes. By comparing the RMSDs of the backbone atoms for three parallel trajectories shown in Fig. 2, we find each trajectory has a similar trend. In addition, after the initial 2 ns molecular dynamics simulations, most of systems are up to equilibration except S42A mutant. As Fig. 2 shows, S42A mutant becomes to stabilize only after 8 ns. To further analyze the interaction profile, MM-GBSA method was applied to calculate the binding free energy. The snapshot structures used for these calculations were extracted from the equilibrated portions of the selected 10 ns molecular dynamics (MD) trajectory. To keep the consistence of the number of snapshots used for MM-GBSA calculations, only the last 2 ns trajectories for each simulation were used by considering the equilibration time of S42A mutant. Two-hundred snapshots for each trajectory were extracted and used for the enthalpy calculation. Because of the high computational demand, only 20 snapshots were used to calculate the entropy. The calculated average binding free energies and the detailed contribution of various energy components are shown in Tables 1, S1 and S2 in the supporting information. By comparing the binding free energy from the parallel trajectories, it can be seen that each parallel trajectory give similar results except for R35AR46A mutant. From the binding experiments and our results, we know R35AR46A double mutation makes the binding ability of NS1A to dsRNA lose completely (Cheng et al., 2009), indicating that R35AR46A double mutation can change the interaction mode of NS1A and dsRNA on a large scale. In our study, for each mutation, we only performed 10 ns molecular dynamics simulations. The short simulation time cannot echo such large conformational change, which should be responsible for the large difference of binding free energy for R35AR46A mutant for each parallel trajectory.

Because of the similarity of results from each parallel trajectory, here, we focus on the results from the first trajectory of each system. From Table 1, the calculated binding free energy for wild type NS1A is −157.62 kcal/mol, which should be much lower than the experimental results. Generally, MM-GBSA method will give a much negative binding free energy and it is difficult to reproduce the absolute value of the experimental results (Hou et al., 2011; Raju et al., 2010; Strockbine and Rizzo, 2007). However, there are a good correlation between the calculated binding free energy by this method and experimental one (Hou et al., 2011; Raju et al., 2010). In other words, generally, this method can give a good rank of binding free energy for different systems. In this study, our aim

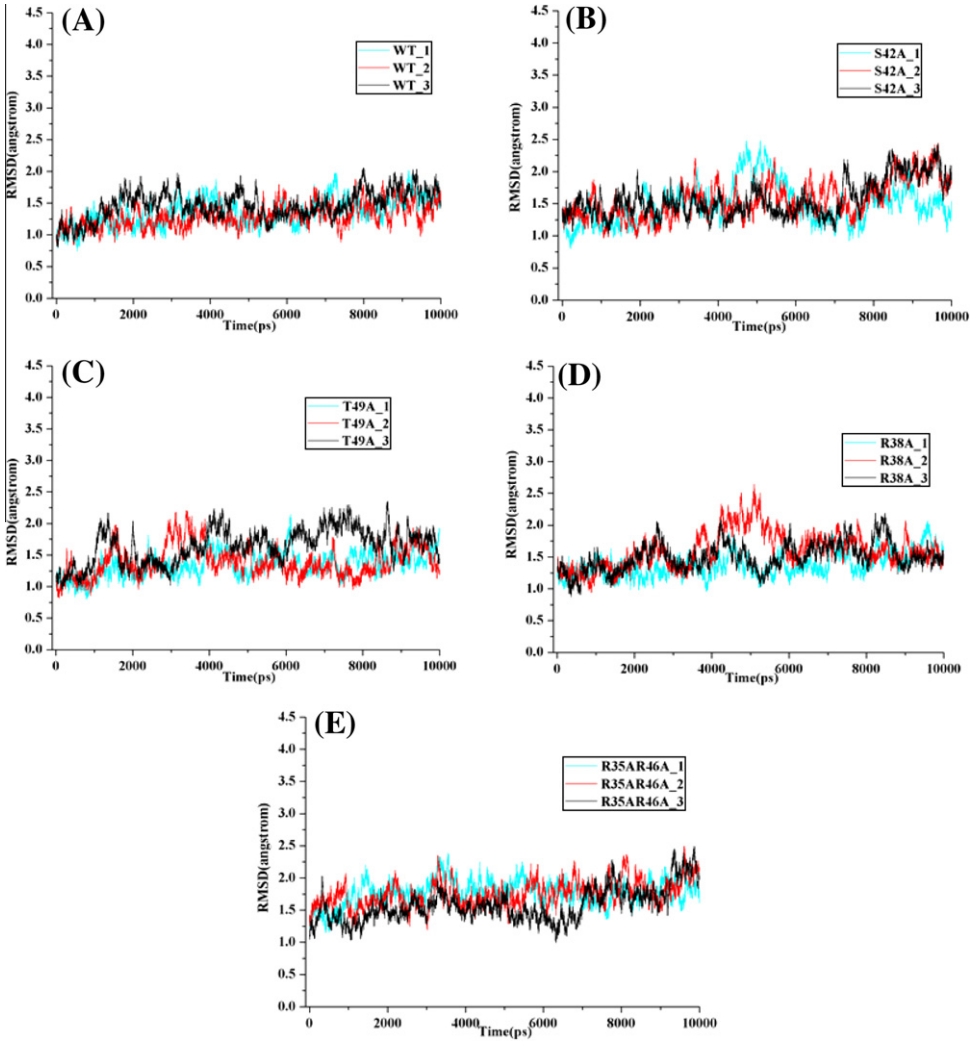

Fig. 2. The monitoring of RMSDs of backbone atoms of the NS1A–dsRNA complexes in three parallel trajectories from the corresponding initial structures: (A) WT; (B) S42A; (C) T49A; (D) R38A; (E) R35AR46A.

Table 1
Calculated binding free energy and its components (kcal/mol) of the wild type and mutated NS1A–dsRNA complexes based on the first group trajectories.

	WT	S42A	T49A	R38A	R35AR46A
ΔE_{ele}	−1231.79	−1200.78	−1217.74	−723.82	−390.76
ΔE_{vdw}	−159.06	−160.19	−150.99	−132.91	−112.15
ΔE_{MM}	−1390.85	−1360.97	−1368.73	−856.73	−502.91
$\Delta G_{sol\text{-}np}$	−21.40	−21.19	−20.55	−18.80	−16.60
$\Delta G_{sol\text{-}ele}$	1190.96	1163.42	1176.73	716.76	397.47
ΔG_{sol}	1169.56	1142.23	1156.18	697.96	380.87
ΔG_{polar} [a]	−40.83	−37.36	−41.01	−7.06	6.71
$\Delta G_{nonpolar}$ [b]	−180.46	−181.38	−171.54	−151.71	−128.75
ΔH_{bind}	−221.29	−218.75	−212.56	−158.78	−122.03
$T\Delta S$	−63.67	−67.13	−61.96	−65.40	−59.98
ΔG_{bind}	−157.62	−151.62	−150.60	−93.38	−62.05

[a] $\Delta G_{polar} = \Delta E_{ele} + \Delta G_{sol\text{-}ele}$.
[b] $\Delta G_{nonpolar} = \Delta E_{vdw} + \Delta G_{sol\text{-}np}$.

is to use MM-GBSA calculations to reveal the sources governing binding and understand how several important mutants reduce or abolish dsRNA binding, rather than to calculate the absolute binding energy. Thus, we care more about the contribution of different energy items and key residues as well as the relative binding energy difference of wild type and mutated NS1A, not the absolute binding free energy. Since MM-GBSA method can give the relative binding energy accurately and have a special advantage to decompose the binding free energy to different energy items and individual residues, it is a much suitable method to be applied in this study.

By decomposing free energy into identifiable contributions, we can understand the origin to determine the binding of NS1A and dsRNA. Enthalpy contributions provide a measure of the strength of the interactions between dsRNA and the protein (electrostatic, van der Waals interactions), relative to those with the solvent. Entropic contributions comprise the change in solvent entropy arising from the burial of hydrophobic groups upon binding and the loss of solute conformational degrees of freedom (translational, rotational, and vibrational). From the Table 1, the change of entropy during the formation of NS1A–dsRNA complex is very large, indicating that the large conformation change occurs for protein and RNA upon the formation of complex. In addition, by analyzing the interface residues of NS1A–dsRNA complex, several hydrophobic residues such as P31, F32, L33 and L36 are buried into the interior of the complex upon binding, which should also contribute to the large entropy change. At the same time, from the perspective of enthalpy, it is highly favorable to the binding of NS1A and dsRNA. Fig. 3 shows the fluctuations of total enthalpy energy over each snapshot. It can be seen that the calculated enthalpy has a small fluctuation in the last 2 ns. From the contribution of individual en-

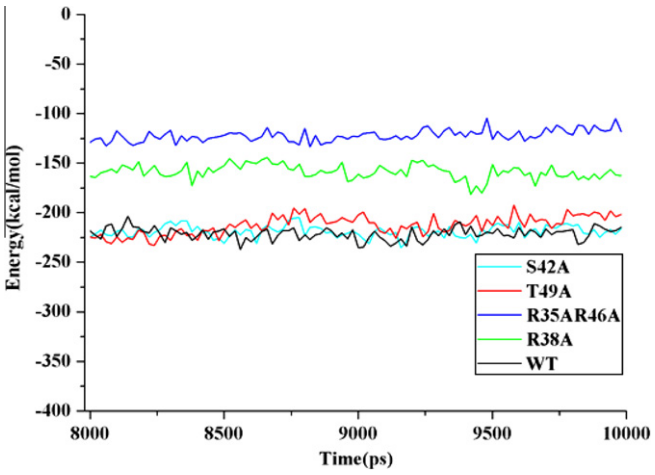

Fig. 3. Time evolution of total enthalpy calculated by MM-GBSA method for all studied systems.

ergy contribution, the nonpolar or hydrophobic interaction ($\Delta G_{nonpolar} = \Delta E_{vdw} + \Delta G_{sol\text{-}np}$) with −180.46 kcal/mol contribution provides the main driving force for binding. Relative to the hydrophobic interaction, the electrostatic interaction ($\Delta G_{polar} = \Delta E_{ele} + \Delta G_{sol\text{-}ele}$) have a smaller but also obvious contribution. Actually, the direct intermolecular electrostatic interactions (ΔE_{ele}) are highly favorable to the binding but their contributions are compensated by the large desolvation penalties ($\Delta G_{sol\text{-}ele}$) associated with the binding process.

To identify the hotspot residues of the protein–RNA interaction interface, pair interaction energy analysis was employed on the first group parallel trajectories and the corresponding results were given in Figs. 4 and 5. From Fig. 4A, we can see that there are 17 residues for NS1A have more than 2 kcal/mol free energy contribution to its binding to dsRNA. Fig. 5 gives a vivid representation for the distribution and contribution of the 17 important residues. Basically, the identified hotspot residues can be classified into two classes according to their distance from the binding site. One class including R19, K20, R21, R59, K62, and R67 is located beyond 6 Å of the binding site, but they can influence the binding process through the indirect interaction. For example, R19 can form strong hydrogen bond with D39. This hydrogen bond is very important for the formation of helix–helix dimmer of NS1A, which helix–helix dimmer plays a critical role on dsRNA binding (Aramini et al., 2011). In addition, R19 can also form one hydrogen bond with backbone carboxyl group of R35. As we know, R35 can form the direct and important interactions with dsRNA. Others residues including M1 and residues 31–49 lie in the binding surface and they can form the direct interaction with dsRNA. These indirect and direct interactions form the recognition basis of dsRNA and NS1A. Among these residues, five residues including M1, R35, R38, K41 and R46 are especially important with more than 5 kcal/mol free energy contributions. For dsRNA, mainly two regions have important contributions for binding process due to having close contact region with the protein. One important region consists of bases C4, A5, G6, C7 and A8. The other region includes three bases from G16 to C18.

Some of our identified important residues based on binding free energy calculations have been proved to be critical for NS1A–dsRNA binding from experiments. For example, the R38 with a largest contribution in our calculation to dsRNA binding has been proved to be the only necessary amino acid residue absolutely required for dsRNA binding (Min and Krug, 2006). In addition, isothermal titration calorimetric (ITC) assay showed that R35AR46A double mutations abolished dsRNA binding completely (Cheng et al., 2009). In our calculation, both R35 and R46 residues have more than 7 kcal/mol binding energy binding contribution. From ITC assay, S42A and T49A mutations decrease the dsRNA-binding affinity by 10-fold. The involved two residues S42 and T49 are shown to be with more than 2 kcal/mol contribution from pair interaction energy analysis. These facts indicate the free energy calculations are in a good agreement with experimental assay and can identify the hot spot residues of protein–RNA interface.

To search the source of the large contribution from the key residues, we further perform a more detailed analysis of the intermolecular interactions on these residues. The intermolecular interaction can be divided into polar and nonpolar interaction generally. As for protein–RNA complex, the polar interaction mainly includes the electrostatic interaction in gas phase and the polar solvation free energy. By analyzing the contribution of individual energy during the process of NS1A–dsRNA complex formation, the nonpolar or hydrophobic interaction ($\Delta G_{nonpolar} = \Delta E_{vdw} + \Delta G_{sol\text{-}np}$) has −180.46 kcal/mol contribution and the polar interaction ($\Delta G_{polar} = \Delta E_{ele} + \Delta G_{sol\text{-}ele}$) has −40.83 kcal/mol contribution. The absolute value of individual energy contribution is not critical. We care more about which residues should be responsible for each energy terms. To answer this question, the contribution of the identified seventeen key residues is further decomposed into polar and nonpolar section in Fig. 6. From Fig. 6, it can be seen that most of important residues for NS1A have a large polar interaction contribution while the identified most important five residues M1, R35, R38, K41 and R46 have obvious contributions both from polar and nonpolar interactions. However for other residues, only single contribution of polar or nonploar interaction play an important role for NS1A binding to RNA. For example, two relative important residues S42 and T49, whose mutation into alanine will decrease the dsRNA-binding affinity by 10-fold, display their contribution to binding process only from the nonpolar interaction.

3.2. The origin of binding affinity loss for several reported mutants

Although through the decomposition of binding free energy to every residue, we can identify the hotspot residues of NS1A interface for RNA binding. The above experiments cannot give us the exact reasons of the reduced binding affinity for several reported mutants. How will the R38A single mutation and R35AR46A double mutations abolish dsRNA binding completely? Here, in order to explore the origin of binding affinity loss for the reported mutants, we designed several other simulation systems including S42A, T49A, R38A, R35AR46A and performed three parallel 10 ns molecular dynamics simulations for each system.

Firstly, to monitor the equilibration of trajectory and compare the structural differences, we analyzed the time evolution of RMSD of backbone atoms and calculated the RMS fluctuations of backbone atoms averaged for each residue in NS1A (shown in Figs. 2 and 7). The average RMSD of backbone atoms for wild type, S42A, T49A, R38A and R35AR46A are 1.35 Å, 1.49 Å, 1.34 Å, 1.37 Å, 1.77 Å, respectively. It can be seen that the mutants except R35AR46A have a small and similar RMSD to wild type, indicating that the equilibrated structures are very similar to the crystal structure and the involved mutations do not change the backbone structure largely. For R35AR46A mutant, the relative higher RMSD indicates much larger structural changes happened. The RMSF (root-mean-square fluctuation) analysis (shown in Fig. 7) further indicates the double mutations R35AR46A will make both the protein and RNA more flexible. In details, all the interface residues including residues from 29 to 49 of NS1A and bases from 5 to 13 of RNA have an obvious higher RMSF than that of wild type system, suggesting that the double mutations R35AR46A do disturb the binding of NS1A–dsRNA largely. By comparing the RMSF from other mutants and wild type, the mutated NS1A has similar or a

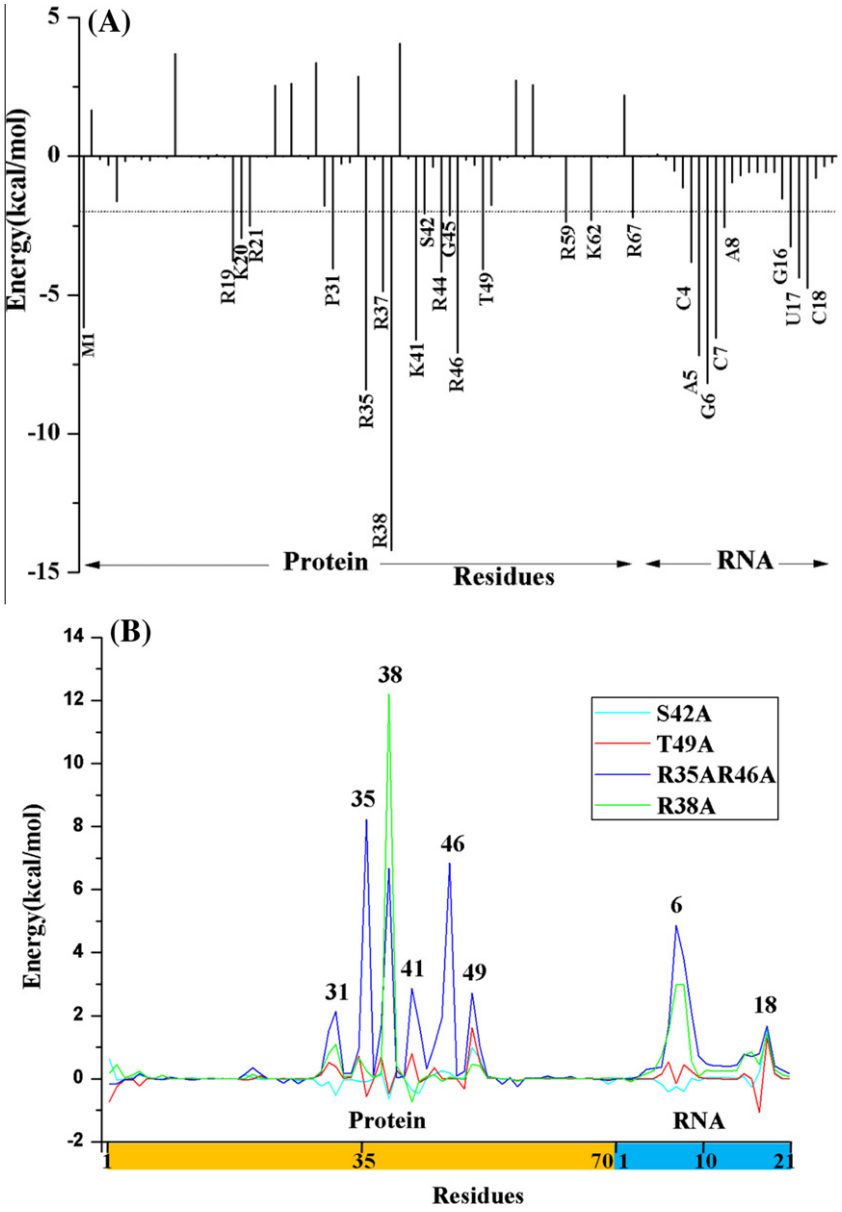

Fig. 4. Pair interaction energy analysis in NS1A–dsRNA complex: (A) The contribution of each residue to wild type NS1A–dsRNA binding; (B) the energy difference of each residue contribution to binding to the dsRNA for the mutated NS1A–dsRNA complexes relative to wild type one.

little larger RMSF on the close contact region of NS1A protein with dsRNA, indicating that the involved mutations will make the interface residues more flexible and reduce the binding of NS1A and dsRNA slightly.

Based on the last 2 ns trajectory for the studied mutants, we also calculated the binding free energy and the individual energy contribution to the binding of NS1A with dsRNA by using MM-GBSA method. The results were shown in Tables 1, S1 and S2 in the supporting information. As expected, the mutated systems have a smaller binding free energy compared with wild type. The binding free energy of wild type, S42A, T49A, R38A, R35AR46A are −157.62 kcal/mol, −151.62 kcal/mol, −150.60 kcal/mol, −93.38 kcal/mol, and −62.05 kcal/mol, respectively. The dsRNA binding potencies towards the WT and mutated NS1A can be ranked as: WT > S42A > T49A > R38A > R35AR46A according to the order of bind free energies. This rank is well consistent with the experimental result. As reported in the reference, the mutants S42A and T49A decrease the dsRNA binding affinity by only 10-fold. Whereas, R35AR46A double mutations or a single mutation R38A abolish dsRNA binding completely (Cheng et al., 2009).

By comparing the individual energy contribution for wild type and different mutants, we could find out the origin of binding affinity loss for the studied mutants. From Table 1, it can be seen that both the polar and nonpolar contributions of binding energies reduced largely for the R38A and R35AR46A mutants compared with the wild type system. For example, the polar interaction contribution including the direct electrostatic interaction and polar desolvation penalty decreased 33.77 kcal/mol and 47.54 kcal/mol as well as the nonpolar contribution decreased 28.75 kcal/mol and 51.71 kcal/mol, respectively for the R38A and R35AR46A mutants relative to the wild type NS1A. As for the S42A mutant, only the polar contribution shows a slight decline. On the contrary, only nonpolar contribution reduces with 8.92 kcal/mol for T49A mutant.

In order to explore which residues are responsible for the reduced binding free energy for the studied mutants, we further decompose the binding free energy to per residue and plot the

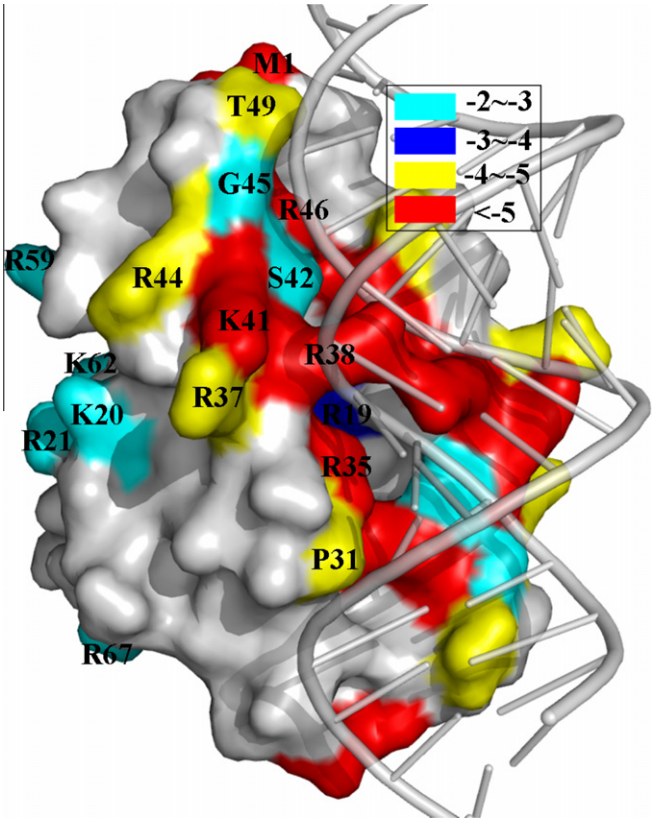

Fig. 5. The hotspot residues of NS1A surface and their corresponding energy contributions (kcal/mol).

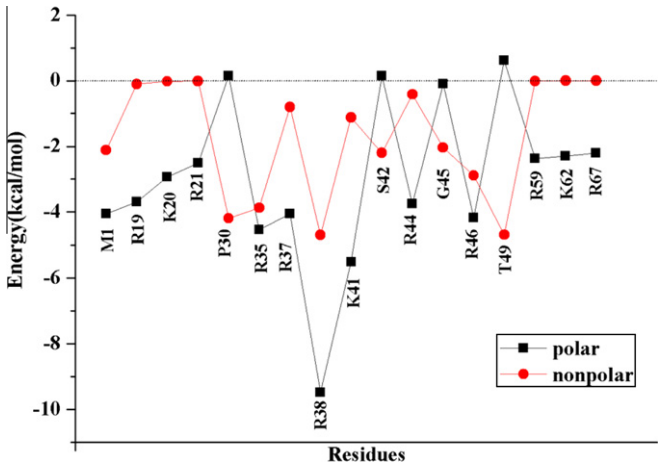

Fig. 6. The polar and nonpolar interaction contributions for the identified key residues of NS1A.

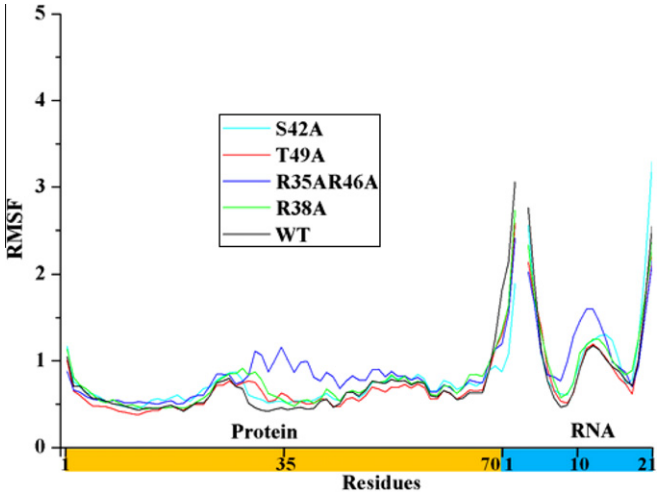

Fig. 7. The RMSFs relative to the initial structure for backbone atoms of the NS1A–dsRNA complexes.

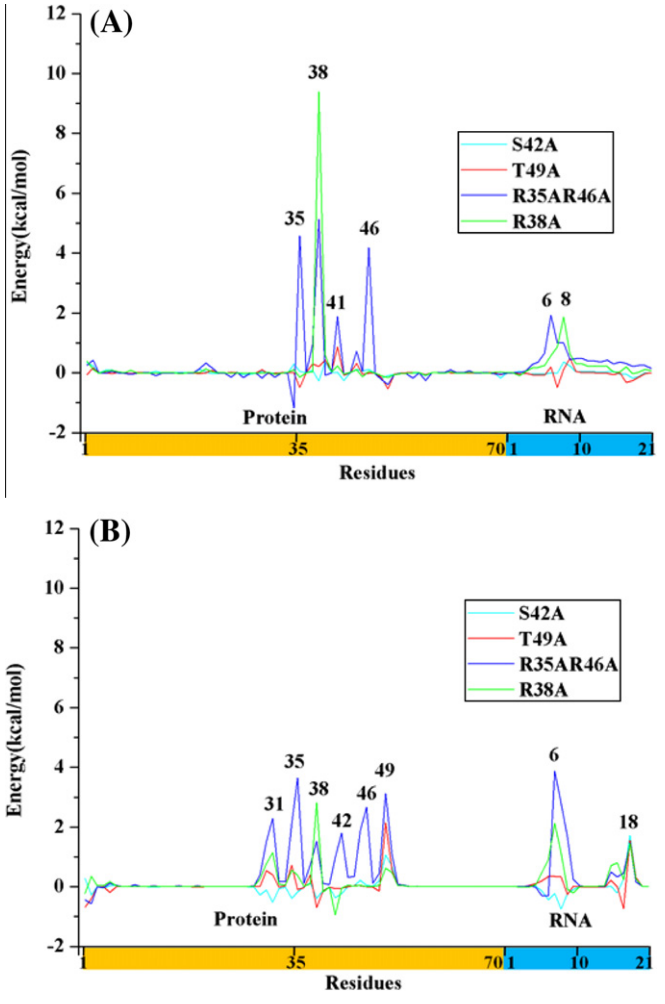

Fig. 8. Energy contribution difference of each residue for the mutated NS1A–dsRNA binding relative to the wild type NS1A–dsRNA binding: (A) The polar contribution; (B) the nonpolar contribution.

contribution difference of per residue for mutated and wild type NS1A in Fig. 4B. Here, it needs to be noted that the decomposition of binding free energy is only to the enthalpy contribution without entropy contribution. From Fig. 4B, except R35AR46A mutant, basically, only the involved mutated residues are responsible for the binding affinity decreasing. For example, the mutation from R38 to A38 makes the free energy contribution of the residue 38 decrease obviously from −14.19 kcal/mol to −1.99 kcal/mol. By analyzing the change of RNA residues' contributions, it can be seen that the binding affinity decreasing of R38A mutant should attribute to the disappearing of the interaction between residue 38 from NS1A and G6-A8 from RNA. Compared with R38A system, the contribution from per residue for S42A and T49A systems has a small difference relatively to that in wild type NS1A since the

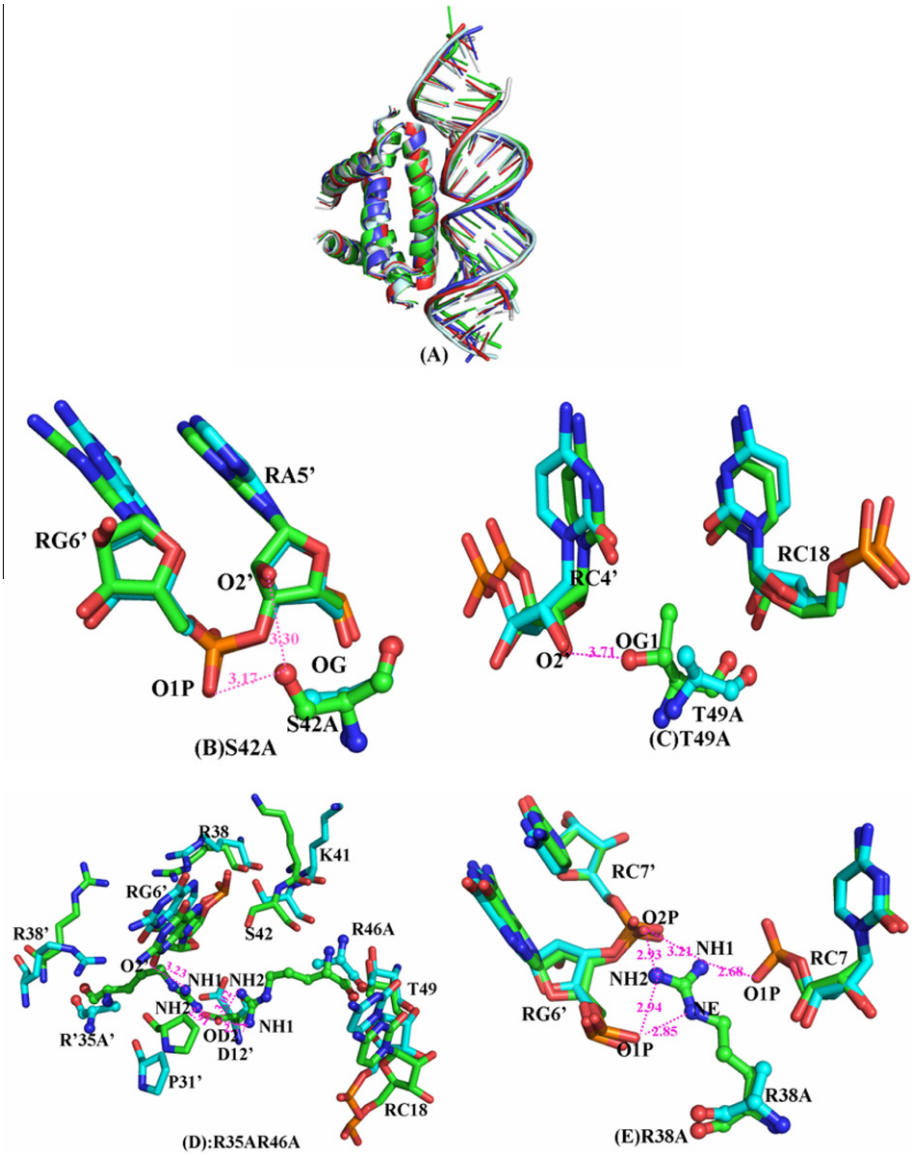

Fig. 9. The representative structures of all studied systems obtained from the clustering analysis based on 10 ns trajectory: (A) the representative structures of the mutants aligned to the wild type structure (the representative structures of S42T, T49A, R35AR46A, R38A, and WT NS1A are colored by cyan, red, blue, green, white respectively); (B–E) the comparison of key interactions between the wild type and studied mutants (carbon atoms of all the mutants are colored by blue, carbon atoms of wild type system are colored by green); (B) S42A; (C) T49A; (D) R35AR46A; (E) R38A. (For interpretation of the references to color in this figure legend, the reader is referred to the web version of this article.)

two mutations give a slight effect to NS1A binding to RNA wholly. As for the R35AR46A double mutants, not only the mutated residues but also other residues such as P31, R38, S42 and T49 exert the obvious reduced contribution for NS1A binding to RNA, indicating that the double mutations interfere the formation of complex wholly. This is consistent with the above RMSF analysis and experimental results.

To search the origin of the loss of the above residues' contribution, we further analyze the difference of per-residue polar and nonpolar contributions between the mutated and wild type system and give the corresponding results in Fig. 8. From Fig. 8, for R38A mutant, the loss of polar contribution of residue 38 is the main reason of the binding affinity decreasing. In wild type NS1A, R38 penetrates into dsRNA helix and the three nitrogen atoms of its side chain form hydrogen bonds with the oxygen atoms from phosphate of four bases, including G6, C7 in one strand and C7, A8 in the other strand. From R38 to A38, all these hydrogen bonds disappear completely, leading to a large reduce of polar interaction. In addition, the side chain penetrating into RNA helix also forms the strong vdw interaction by the packing of side chain from R38 with RNA residues. The loss of packing of the side chain results in the obvious decline of the nonpolar interaction for residue 38 from NS1A and G6 from RNA. In order to explore the structural detail changes between mutant and wild type system, clustering analysis were applied to extract the conformation that best represents the whole ensemble. During the clustering analysis, the self-organization map method from the AMBER ptraj module was used to cluster the MD trajectories based on the pairwise similarity measured by the backbone atoms root-mean square deviation. The largest cluster was chosen and shown in Fig. 9. From Fig. 9A, there are no significant changes for backbone atoms in the R38A mutant compared to wild type structure indicating that this mutation has a small influence on the overall structure of NS1A–dsRNA. By focusing on the change of the side chains for R38A mutation (Fig. 9E), we can see clearly that the mutation from a large and polar residue arginine to a small and neural residue alanine makes

the important interactions which take a primary role to anchor dsRNA and keep dsRNA binding to NS1A well, disappear entirely, resulting in a large decreasing of dsRNA binding affinity to protein.

For S42A mutant, due to the small difference (2.54 kcal/mol) of enthalpy compared with wild type system totally, it is difficult to see the obvious fall for the polar and nonpolar contribution of the special residue. As for T49A system, the loss of nonpolar contribution of residue 49 from NS1A and C18 from RNA should be responsible for the binding affinity decreasing. The structural analysis from Fig. 9A–C also shows that the two mutations do not influence the overall structure of NS1A–dsRNA and only small change of side chain occurred.

From Fig. 8, for the R35AR46A double mutants, a large decrease of binding affinity is from both the loss of polar contribution from the residues A35, R38, S42, A46 and the loss of nonpolar contribution from residues P31, A35, R38, S42, A46, T49 from NS1A. Correspondingly, the interfacial residues 6–10 of RNA especially G6 show the obvious decreased polar and nonpolar contributions. Almost all interfacial residues' reduced contributions indicate that the simultaneous mutation of pairs of Arg35–Arg46 sharpens the influence of single mutation to binding affinity of NS1A and dsRNA. The structural analysis further proves the large effect of the double mutations. From Fig. 9A, it can be seen that the RNA structure distorts on some degree. In Fig. 9D, we compared the detailed interaction difference of the side chains in wild type and R35AR46A system. In wild type NS1A, the positively charged residues Arg35 and Arg46 have important contributions to dsRNA binding through the formation of hydrogen bonds and salt bridges. The mutations of R35 and R46 to alanine make such strong electrostatic interaction disappeared largely. The simultaneous disappearing of several pairs of key hydrogen bonds and salt bridges to anchor dsRNA makes the binding of NS1A–dsRNA very unstable as well as the subsequent impair interactions of the interfacial residues further aggravate this instability.

4. Conclusions

In this study, we combined multiple trajectories molecular dynamics simulation and binding free energy calculation to explore the essence of NS1A–RNA interaction, which is a promising anti-influenza target. Based on the results from MM-GBSA, the nonpolar interaction has a more important contribution than polar interaction to dsRNA binding to NS1A protein. However, by comparing the individual energy contributions of the mutated and wild type systems, the origin of decrease of binding affinity for different mutants is different. For R38A and R35AR46A mutants, both the polar and nonpolar contributions reduced largely compared with the wild type system. For S42A mutant, only the polar contribution shows a slight decline. On the contrary, only nonpolar contribution reduced for T49A mutant. Through the decomposition of free energy to per-residue, 17 key residues are identified to be important for NS1A–RNA interaction. All the key residues identified by experiments are included in our key residues group. The simulation of several reported mutants indicates the mutations have a small effect to the backbone structures but the loss of side chain interactions is responsible for binding affinity decrease. The detailed understanding of NS1A–dsRNA interaction can provide some insights for the structure-based design or discovery of novel antivirus drugs and will be useful for human being to fight against influenza.

Acknowledgments

This work was supported by the National Natural Science Foundation of China (Grant Nos.: 21103075 and 21175063) and the Fundamental Research Funds for the Central Universities (Grant No.: lzujbky-2011-t01). We would like to thank the Gansu Computing Center for providing the computing resources.

Appendix A. Supplementary data

Supplementary data associated with this article can be found, in the online version, at doi:10.1016/j.antiviral.2011.09.009.

References

Aramini, J.M., Ma, L.C., Zhou, L., Schauder, C.M., Hamilton, K., Amer, B.R., Mack, T.R., Lee, H.W., Ciccosanti, C.T., Zhao, L., Xiao, R., Krug, R.M., Montelione, G.T., 2011. Dimer interface of the effector domain of non-structural protein 1 from influenza A virus: an interface with multiple functions. J. Biol. Chem. 286, 26050–26060.

Case, D.A., Cheatham 3rd, T.E., Darden, T., Gohlke, H., Luo, R., Merz Jr., K.M., Onufriev, A., Simmerling, C., Wang, B., Woods, R.J., 2005. The amber biomolecular simulation programs. J. Comput. Chem. 26, 1668–1688.

Cheng, A., Wong, S.M., Yuan, Y.A., 2009. Structural basis for dsRNA recognition by NS1 protein of influenza A virus. Cell Res. 19, 187–195.

Chien, C.Y., Tejero, R., Huang, Y., Zimmerman, D.E., Rios, C.B., Krug, R.M., Montelione, G.T., 1997. A novel RNA-binding motif in influenza A virus non-structural protein 1. Nat. Struct. Biol. 4, 891–895.

Chien, C.Y., Xu, Y., Xiao, R., Aramini, J.M., Sahasrabudhe, P.V., Krug, R.M., Montelione, G.T., 2004. Biophysical characterization of the complex between double-stranded RNA and the N-terminal domain of the NS1 protein from influenza A virus: evidence for a novel RNA-binding mode. Biochemistry 43, 1950–1962.

Chong, L.T., Duan, Y., Wang, L., Massova, I., Kollman, P.A., 1999. Molecular dynamics and free-energy calculations applied to affinity maturation in antibody 48G7. Proc. Natl. Acad. Sci. USA 96, 14330–14335.

Das, K., Aramini, J.M., Ma, L.C., Krug, R.M., Arnold, E., 2010. Structures of influenza A proteins and insights into antiviral drug targets. Nat. Struct. Mol. Biol. 17, 530–538.

Das, K., Ma, L.C., Xiao, R., Radvansky, B., Aramini, J., Zhao, L., Marklund, J., Kuo, R.L., Twu, K.Y., Arnold, E., Krug, R.M., Montelione, G.T., 2008. Structural basis for suppression of a host antiviral response by influenza A virus. Proc. Natl. Acad. Sci. USA 105, 13093–13098.

de Jong, M.D., Tran, T.T., Truong, H.K., Vo, M.H., Smith, G.J., Nguyen, V.C., Bach, V.C., Phan, T.Q., Do, Q.H., Guan, Y., Peiris, J.S., Tran, T.H., Farrar, J., 2005. Oseltamivir resistance during treatment of influenza A (H5N1) infection. N. Engl. J. Med. 353, 2667–2672.

DeLano, W.L., 2002. The PyMOL Molecular Graphics System. <http://www.pymol.org>.

Dharan, N.J., Gubareva, L.V., Meyer, J.J., Okomo-Adhiambo, M., McClinton, R.C., Marshall, S.A., St George, K., Epperson, S., Brammer, L., Klimov, A.I., Bresee, J.S., Fry, A.M., 2009. Infections with oseltamivir-resistant influenza A (H1N1) virus in the United States. JAMA 301, 1034–1041.

Essmann, U., Perera, L., Berkowitz, M.L., Darden, T., Lee, H., Pedersen, L.G., 1995. A smooth particle mesh Ewald method. J. Chem. Phys. 103, 8577–8593.

Hale, B.G., Randall, R.E., Ortin, J., Jackson, D., 2008. The multifunctional NS1 protein of influenza A viruses. J. Gen. Virol. 89, 2359–2376.

Hartley, D.M., Nelson, N.P., Perencevich, E.N., 2009. Antiviral drugs for treatment of patients infected with pandemic (H1N1) 2009 virus. Emerg. Infect. Dis. 15, 1851–1852.

Hatada, E., Fukuda, R., 1992. Binding of influenza A virus NS1 protein to dsRNA in vitro. J. Gen. Virol. 73 (Pt 12), 3325–3329.

Hay, A.J., Wolstenholme, A.J., Skehel, J.J., Smith, M.H., 1985. The molecular basis of the specific anti-influenza action of amantadine. EMBO J. 4, 3021–3024.

Hou, T., Wang, J., Li, Y., Wang, W., 2011. Assessing the performance of the MM/PBSA and MM/GBSA methods. 1. The accuracy of binding free energy calculations based on molecular dynamics simulations. J. Chem. Inf. Model 51, 69–82.

Hurt, A.C., Holien, J.K., Parker, M., Kelso, A., Barr, I.G., 2009. Zanamivir-resistant influenza viruses with a novel neuraminidase mutation. J. Virol. 83, 10366–10373.

Jorgensen, W.L., Chandrasekhar, J., Madura, J.D., Impey, R.W., Klein, M.L., 1983. Comparison of simple potential functions for simulating liquid water. J. Chem. Phys. 79, 926–935.

Kim, C.U., Lew, W., Williams, M.A., Liu, H., Zhang, L., Swaminathan, S., Bischofberger, N., Chen, M.S., Mendel, D.B., Tai, C.Y., Laver, W.G., Stevens, R.C., 1997. Influenza neuraminidase inhibitors possessing a novel hydrophobic interaction in the enzyme active site: design, synthesis, and structural analysis of carbocyclic sialic acid analogues with potent anti-influenza activity. J. Am. Chem. Soc. 119, 681–690.

Kollman, P.A., Massova, I., Reyes, C., Kuhn, B., Huo, S., Chong, L., Lee, M., Lee, T., Duan, Y., Wang, W., Donini, O., Cieplak, P., Srinivasan, J., Case, D.A., Cheatham 3rd, T.E., 2000. Calculating structures and free energies of complex molecules: combining molecular mechanics and continuum models. Acc. Chem. Res. 33, 889–897.

Krug, R.M., Aramini, J.M., 2009. Emerging antiviral targets for influenza A virus. Trends Pharmacol. Sci. 30, 269–277.

Krug, R.M., Yuan, W., Noah, D.L., Latham, A.G., 2003. Intracellular warfare between human influenza viruses and human cells: the roles of the viral NS1 protein. Virology 309, 181–189.

Le, Q.M., Kiso, M., Someya, K., Sakai, Y.T., Nguyen, T.H., Nguyen, K.H., Pham, N.D., Ngyen, H.H., Yamada, S., Muramoto, Y., Horimoto, T., Takada, A., Goto, H., Suzuki, T., Suzuki, Y., Kawaoka, Y., 2005. Avian flu: isolation of drug-resistant H5N1 virus. Nature 437, 1108.

Liu, H., Yao, X., 2010. Molecular basis of the interaction for an essential subunit PA-PB1 in influenza virus RNA polymerase: insights from molecular dynamics simulation and free energy calculation. Mol. Pharmaceut. 7, 75–85.

Liu, J., Lynch, P.A., Chien, C.Y., Montelione, G.T., Krug, R.M., Berman, H.M., 1997. Crystal structure of the unique RNA-binding domain of the influenza virus NS1 protein. Nat. Struct. Biol. 4, 896–899.

Liu, Y., Zhang, J., Xu, W., 2007. Recent progress in rational drug design of neuraminidase inhibitors. Curr. Med. Chem. 14, 2872–2891.

Lu, Y., Wambach, M., Katze, M.G., Krug, R.M., 1995. Binding of the influenza virus NS1 protein to double-stranded RNA inhibits the activation of the protein kinase that phosphorylates the eIF-2 translation initiation factor. Virology 214, 222–228.

Min, J.Y., Krug, R.M., 2006. The primary function of RNA binding by the influenza A virus NS1 protein in infected cells: inhibiting the 2′-5′ oligo (A) synthetase/RNase L pathway. Proc. Natl. Acad. Sci. USA 103, 7100–7105.

Mishin, V.P., Hayden, F.G., Gubareva, L.V., 2005. Susceptibilities of antiviral-resistant influenza viruses to novel neuraminidase inhibitors. Antimicrob. Agents Chemother. 49, 4515–4520.

Moscona, A., 2009. Global transmission of oseltamivir-resistant influenza. N. Engl. J. Med. 360, 953–956.

Nemeroff, M.E., Barabino, S.M., Li, Y., Keller, W., Krug, R.M., 1998. Influenza virus NS1 protein interacts with the cellular 30 kDa subunit of CPSF and inhibits 3'end formation of cellular pre-mRNAs. Mol. Cell. 1, 991–1000.

Noah, D.L., Twu, K.Y., Krug, R.M., 2003. Cellular antiviral responses against influenza A virus are countered at the posttranscriptional level by the viral NS1A protein via its binding to a cellular protein required for the 3′ end processing of cellular pre-mRNAS. Virology 307, 386–395.

Raju, R.K., Burton, N.A., Hillier, I.H., 2010. Modelling the binding of HIV-reverse transcriptase and nevirapine: an assessment of quantum mechanical and force field approaches and predictions of the effect of mutations on binding. Phys. Chem. Chem. Phys. 12, 7117–7125.

Rungrotmongkol, T., Frecer, V., De-Eknamkul, W., Hannongbua, S., Miertus, S., 2009. Design of oseltamivir analogs inhibiting neuraminidase of avian influenza virus H5N1. Antiviral Res. 82, 51–58.

Russell, R.J., Haire, L.F., Stevens, D.J., Collins, P.J., Lin, Y.P., Blackburn, G.M., Hay, A.J., Gamblin, S.J., Skehel, J.J., 2006. The structure of H5N1 avian influenza neuraminidase suggests new opportunities for drug design. Nature 443, 45–49.

Ryckaert, J.-P., Ciccotti, G., Berendsen, H.J.C., 1977. Numerical integration of the cartesian equations of motion of a system with constraints: molecular dynamics of n-alkanes. J. Comput. Phys. 23, 327–341.

Sharon, A., Balaraju, T., Bal, C., 2011. A catalytic 3D model development of HIV-integrase and drug resistance understanding by molecular dynamics simulation. Antiviral Res. 90, A43–A44.

Sitkoff, D., Sharp, K.A., Honig, B., 1994. Accurate calculation of hydration free energies using macroscopic solvent models. J. Phys. Chem. 98, 1978–1988.

Solorzano, A., Webby, R.J., Lager, K.M., Janke, B.H., Garcia-Sastre, A., Richt, J.A., 2005. Mutations in the NS1 protein of swine influenza virus impair anti-interferon activity and confer attenuation in pigs. J. Virol. 79, 7535–7543.

Srinivasan, J., Cheatham, T.E., Cieplak, P., Kollman, P.A., Case, D.A., 1998. Continuum solvent studies of the stability of DNA, RNA, and phosphoramidate–DNA helices. J. Am. Chem. Soc. 120, 9401–9409.

Stouffer, A.L., Acharya, R., Salom, D., Levine, A.S., Di Costanzo, L., Soto, C.S., Tereshko, V., Nanda, V., Stayrook, S., DeGrado, W.F., 2008. Structural basis for the function and inhibition of an influenza virus proton channel. Nature 451, 596–599.

Strockbine, B., Rizzo, R.C., 2007. Binding of antifusion peptides with HIVgp41 from molecular dynamics simulations: quantitative correlation with experiment. Proteins 67, 630–642.

von Itzstein, M., Wu, W.Y., Kok, G.B., Pegg, M.S., Dyason, J.C., Jin, B., Van Phan, T., Smythe, M.L., White, H.F., Oliver, S.W., et al., 1993. Rational design of potent sialidase-based inhibitors of influenza virus replication. Nature 363, 418–423.

Wang, C., Takeuchi, K., Pinto, L.H., Lamb, R.A., 1993. Ion channel activity of influenza A virus M2 protein: characterization of the amantadine block. J. Virol. 67, 5585–5594.

Wang, W., Riedel, K., Lynch, P., Chien, C.Y., Montelione, G.T., Krug, R.M., 1999. RNA binding by the novel helical domain of the influenza virus NS1 protein requires its dimer structure and a small number of specific basic amino acids. RNA 5, 195–205.

Weinstock, D.M., Zuccotti, G., 2009. The evolution of influenza resistance and treatment. JAMA 301, 1066–1069.